Locally monochromatic two-step nonlinear trident process in a plane wave

S. Tang[1] and B. King[2,3,*]

[1]*College of Physics and Optoelectronic Engineering, Ocean University of China, Qingdao, Shandong, 266100, China*
[2]*Deutsches Elektronen-Synchrotron DESY, Notkestrasse 85, 22607 Hamburg, Germany*
[3]*Centre for Mathematical Sciences, University of Plymouth, Plymouth, PL4 8AA, United Kingdom*

(Received 2 December 2022; accepted 18 April 2023; published 8 May 2023)

In many-cycle plane waves at intermediate intensities, the nonlinear trident process can be well approximated by the two sequential steps of nonlinear Compton scattering of a polarized real photon followed by its transformation into an electron-positron pair via nonlinear Breit-Wheeler pair creation. We investigate this two-step process in the intermediate intensity regime by employing the locally monochromatic approximation for each step and numerically evaluating resulting expressions. When photon polarization is included, it is found to produce an order 10% decrease in the trident rate: the importance of polarization increases at lower intensities, and decreases at higher intensities. Its importance persists at higher intensities in a linearly polarized background, but disappears at high intensities in a circularly polarized background. If the two steps are made to take place in two linearly polarized plane wave pulses with perpendicular polarizations, the pair yield can be increased by approximately 30% compared to two plane waves with the same polarization. It is also shown that harmonic structures in the Compton step can be passed to the pair step if the Compton edge is at an energy of the order of the threshold for linear Breit-Wheeler.

DOI: 10.1103/PhysRevD.107.096004

I. INTRODUCTION

In sufficiently intense electromagnetic backgrounds, quantum electrodynamics (QED) becomes nonlinear and all orders of interaction between charges and the background must be taken into account. "Nonlinear" Compton scattering then, can involve many interactions with some intense and (typically) low-energy background in the process of a charge emitted a single, high-energy photon. In the landmark E144 experiment at SLAC in the mid 1990s, a 46.6 GeV electron beam was collided with a weakly focused laser of moderate intensity parameter ($\xi \approx 0.3$) in a near head-on collision [1–3]. This provided the first measurement of nonlinear Compton scattering (NLC) of real high energy photons and their transformation into electron-positron pairs via the nonlinear Breit-Wheeler (NBW) process in the multiphoton regime. This sequence of processes is the "two-step" part of the nonlinear trident process $e^{\pm} \to e^{\pm} + e^{+}e^{-}$. Recently, the NA63 experiment at CERN measured the two-step *nonlinear* trident process with $\xi \sim O(10)$, at strong-field parameter $\chi \approx 2.4$ in the collision of 200 GeV electrons with germanium single crystals [4]. It is planned, at the E320 experiment at SLAC [5] and the LUXE experiment at DESY [6], to measure this two-step process in the intermediate intensity regime $\xi \sim O(1)$. Since the intensity parameter represents the charge-field coupling, these new experiments will probe strong-field quantum electrodynamics (QED) effects where the charge-field interaction is nonperturbative and can no longer be described using leading-order multiphoton contributions.

Although exact solutions for the complete nonlinear trident process have been calculated in a plane wave pulse [7–13] also including radiation reaction [13] (as well as in a constant crossed field [14–18], a magnetic field [19], a Coulomb field [20] and also studied using an adiabatic approximation [21] and in trains of laser pulses [22]), they are computationally expensive and a more efficient and versatile method is required to model experiments. Therefore, a simulational approach that calculates particle trajectories classically, and adds first-order QED effects such as the NLC and NBW processes via Monte-Carlo methods, is typically favored in designing and analyzing experiments [3,5,6,23–26]. For second (and higher) order processes, the correct factorization of the n-step subprocess

*b.king@plymouth.ac.uk

requires taking into account the polarization of intermediate particles. For the nonlinear trident process, this means the polarization of the intermediate photon must be included in the NLC and NBW steps [15]. The inclusion of photon polarized strong-field QED processes into simulational approaches is a relatively recent development [4,27–31] and is so far achieved using the locally constant field approximation (LCFA) [32–34]. However, at intermediate intensity values $\xi \sim O(1)$, the LCFA for the first-order processes is known to become inaccurate for typical experimental parameters [35–39].

In the current paper, we assess the importance of photon polarization in modeling the two-step nonlinear trident process. This is achieved by adapting the locally monochromatic approximation (LMA) [40–42], which is being used to model the interaction-point physics of the LUXE experiment [6] as well as strong-field QED experiments at the BELLA PW laser [43] (also appearing in other forms [44,45] and being used in the modeling of the E144 experiment [3]), to include photon-polarized rates for the NLC and NBW processes. Photon polarization has been studied in NLC in monochromatic backgrounds [46] and in plane-wave pulses [47,48]; photon polarization in NBW in the LMA and in plane-wave backgrounds has also been studied [49,50]; the total probability of the photon-polarized trident process in the LMA in a circularly polarized background has also recently been studied [51]; here we gather and present the LMA formulas in a circularly polarized and linearly polarized background. A second focus of this paper is to consider the role of harmonics: whether the harmonic structure of nonlinear Compton, which is a key experimental observable, e.g. in LUXE, can be found in the pair spectrum in the nonlinear trident process. The LMA was chosen as it has been shown that first-order subprocesses can be described more accurately at intermediate intensity values, which are planned to be used in upcoming experiments [41,42]. Although it is known that there are effects missed by the LMA that are related to the finite bandwidth of the background pulse, such as harmonic broadening, low-energy photons produced in NLC [52] and pairs created by the low intensity part of the pulse [53], these should be negligible for realistic set-ups with the parameters we consider here. (For more background on strong-field QED, we direct the reader to the reviews [32,34,54,55].)

This paper is organized as follows. In Sec. II the results are presented for the two-step nonlinear trident process in a circularly polarized (Sec. II A) and a linearly polarized (Sec. II B) background. The results are discussed in Sec. III and conclusions drawn in Sec. IV. Appendix A contains further details about bandwidth effects in the LMA, and in Appendix B, the LMA formulas for photon-polarized nonlinear Compton scattering and photon-polarized nonlinear Breit-Wheeler are given. Finally, in Appendix C, Table I of common parameters is given.

II. LMA FOR TWO-STEP TRIDENT PROCESS

In this section, we combine the LMA formulas (shown in Appendix B) for the NLC and NBW processes [40,49] to calculate the yield of the two-step trident process.

In an intense background, kinematic channels are opened which are otherwise closed in vacuum. This is due to the background being able to supply energy and momentum to a process. Nonlinear QED processes, as they involve multiple interactions with a background can hence have different kinematics to their perturbative, linear counterparts. Overall, nonlinear trident enabled in a strong field background is a $1 \to 3$ process: $e^{\pm} \to e^{\pm} + e^{+}e^{-}$, but we are also interested in the intermediate steps, which are both $1 \to 2$ processes: $e^{\pm} \to e^{\pm} + \gamma$ followed by $\gamma \to e^{+}e^{-}$, and in the two-step case, we take the photon to be on-shell. In this paper, we assume the initial particle is an electron (analogous conclusions follow for a positron). The total probability will depend on: (i) the incoming particle's energy parameter $\eta = \varkappa \cdot p/m^2$, where $\varkappa$ is the plane wave background wave vector, p is the probe electron momentum, m is the mass of the electron; (ii) the intensity parameter ξ of the background, which will be defined in the following in terms of the gauge potential, and (iii) the number of cycles, N of the background. We mainly focus on the total probability, $\mathsf{P} = \mathsf{P}(\xi, \eta, N)$ and lightfront momentum spectrum of the two-step trident process. The parameter space is large and we will also be studying the impact of photon polarization on the total probability. Therefore, in this paper we will restrict our attention to the most relevant parameter ranges, given below.

The initial particle energy will mainly be chosen to be 16.5 GeV and the laser photon energy to be 1.55 eV (800 nm wavelength), or its third harmonic 4.65 eV. This particle energy is chosen as it is the energy of electrons planned to be used at LUXE, and is similar to the energy of 13 GeV used at E320. To investigate higher harmonics, we will calculate one example with 80 GeV and 500 GeV electrons, which are both currently much higher than planned for in experiments. The investigation into potential harmonic structure is particularly relevant for our approach using the LMA, where such effects are captured, in comparison to approaches based on the LCFA, which do not capture harmonic effects. For convenience, in this paper we will use a cosine-squared pulse envelope. We note that this pulse shape has a much wider bandwidth than can be transmitted through optical elements in an experiment. As a consequence, when $\xi \lesssim 1$ and initial electron energies are lower than around 10 GeV, an exact plane-wave calculation will show bandwidth effects beyond the LMA can become dominant. However, these effects will not be present in an experiment. For consistency, we consider initial electron energies higher than this. (See Appendix A for more details on this point.)

The intensity parameter will be varied in the "intermediate regime," $\xi \sim O(1)$, which we take to be $\xi = 0.5 \ldots 5$. This is

significant because the LMA is accurate in this regime, whereas studies of trident based on the LCFA, are limited to higher values of ξ. This parameter regime will also be probed by the E320 and LUXE experiments.

The number of laser cycles N is a less important parameter in the LMA because it can be factored out and occurs just as a preintegral over the laser phase. However, N must be large enough that the LMA is a good approximation to the full QED probability (it is assumed that $N \gg 1$ for this to be the case). We will consider a gauge potential $a = |e|A$ describing the background as a plane wave pulse. The potential depends upon the phase $\phi = \varkappa \cdot x$ in the form:

$$\mathbf{a}^{\perp} = \begin{cases} m\xi f(\phi)(\cos\phi, \varsigma \sin\phi) & |\phi| < \Phi/2 \\ 0 & \text{otherwise,} \end{cases} \tag{1}$$

where $a = (0, \mathbf{a}^{\perp}, 0)$ and $\varsigma \in \{-1, 0, 1\}$ is chosen to switch between linear ($\varsigma = 0$) or circular ($\varsigma = \pm 1$) polarization (we note that the time-averaged amplitude of the potential is different for these two choices). In this paper, we will always use $f(\phi) = \cos^2(\pi\phi/\Phi)$ and $\varsigma = 1$ for circular polarization, where $\Phi = 2\pi N$, and will choose $N = 16$, which corresponds to a full-width-at-half-maximum duration of 21.3 fs for a wavelength of $\lambda = 2\pi/\varkappa^0 = 800$ nm.

Let us denote the lightfront momentum fraction of the photon $s_\gamma = \varkappa \cdot \ell / \varkappa \cdot p$, where ℓ is momentum of photon outgoing from NLC-step and ingoing for NBW-step. The probability for nonlinear Compton scattering of a photon in polarization state σ is P_γ^σ, and nonlinear Breit-Wheeler pair-creation from a photon in the same state is P_e^σ. Then the total probability P for the two-step trident process, can be written [15]:

$$\mathsf{P} = \sum_\sigma \int_0^1 ds_\gamma \int d\phi \frac{d^2\mathsf{P}_\gamma^\sigma(\phi; s_\gamma)}{ds_\gamma d\phi} \mathsf{P}_e^\sigma(\phi; s_\gamma), \tag{2}$$

where $\mathsf{P}_e^\sigma(\phi; s_\gamma) = -\int_\phi d\phi' d\mathsf{P}_e^\sigma(\phi'; s_\gamma)/d\phi'$ and $\sigma \in \{\|, \perp\}$ refers to the two polarization eigenstates of the background. This is depicted in Fig. 1.

For a linearly polarized background, the designation $\|$ ($\perp$) refers to the photon polarization eigenstate being in the same (opposite) polarization state as the background

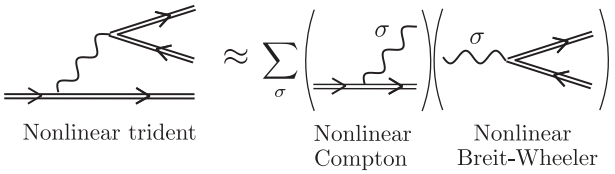

FIG. 1. The nonlinear trident process is approximated as factorized by the sequential processes of nonlinear Compton scattering and nonlinear Breit-Wheeler pair creation involving a real, polarized photon.

with a fixed direction in lab coordinates. For a circularly polarized background, these directions rotate with $\|$ ($\perp$) referring to when a photon collides head-on with the background having a polarization that rotates in the same (opposite) direction as the background.[1] (The polarized NBW probability P_e^σ is defined such that the total unpolarized probability, $\mathsf{P}_e = \mathsf{P}_e^\| + \mathsf{P}_e^\perp$, i.e., the usual 1/2 polarization averaging factor [15] is included already in P_e^σ, and analogously for P_γ^σ.) In order to assess the importance of photon polarization, we will also be interested in the approximation to this probability that uses unpolarized probabilities, P_γ and P_e for the nonlinear Compton and Breit-Wheeler steps respectively. We denote:

$$\tilde{\mathsf{P}} = \int_0^1 ds_\gamma \int d\phi \frac{d^2\mathsf{P}_\gamma(\phi; s_\gamma)}{ds_\gamma d\phi} \mathsf{P}_e(\phi; s_\gamma). \tag{3}$$

(This approximation to the two-step trident probability has often been used in numerical simulations of trident and QED cascades [56–63].) Since the total probability, Eq. (2), involves a sum over polarization eigenstates of the background, to assess the importance of photon polarization, one should consider different background polarization. Here, we study the cases of a circularly and a linearly polarized plane wave pulse.

Probabilities for sub-processes will be calculated within the locally monochromatic approximation [40,49]. This is an adiabatic approximation that neglects derivatives of the slow timescale of the pulse envelope, but includes the fast timescale of the carrier frequency exactly. It can be shown to be equal to the leading order term in an expansion of the total probability in Φ^{-1} [51].

The lightfront momentum is conserved in the interaction with the plane-wave. We use the variable $0 \le s \le 1$ to denote what fraction a particle's lightfront momentum is of the initial electron lightfront momentum. This can be written:

$$1 = s_{e'} + s_\gamma; \qquad s_\gamma = s_q + s_{e''}, \tag{4}$$

where s_γ is the lightfront momentum fraction of the photon, $s_{e'}$ of the scattered electron, $s_{e''}$ of the created electron and s_q of the positron. In this paper, only s_γ and s_q will appear explicitly; the other lightfront momentum fractions will be integrated out. Then we can write the total probability as an integral over the double differential probability:

$$\mathsf{P} = \int_0^1 \mathrm{d}s_q \int_{s_q}^1 \mathrm{d}s_\gamma \frac{\mathrm{d}^2\mathsf{P}}{\mathrm{d}s_q \mathrm{d}s_\gamma}, \tag{5}$$

[1]We note that in terms of helicity states, $\|$ ($\perp$) refer to the photon have the opposite (same) helicity as the background.

where the double differential involves two integrals over the average phase positions of incoming particle in NLC and NBW:

$$\frac{\mathrm{d}^2\mathsf{P}}{\mathrm{d}s_q\mathrm{d}s_\gamma}=\sum_\sigma\int_{\phi_i}^{\phi_f}\mathrm{d}\phi\frac{\mathrm{d}^2\mathsf{P}_\gamma^\sigma(\phi;s_\gamma)}{\mathrm{d}s_\gamma\mathrm{d}\phi}\int_{\phi}^{\phi_f}\mathrm{d}\phi'\frac{\mathrm{d}^2\mathsf{P}_e^\sigma(\phi';s_q)}{\mathrm{d}s_q\mathrm{d}\phi'} \tag{6}$$

(where again $\sigma\in\{\|,\perp\}$). The production of the positron depends not only on the energy of the NLC photon, but also on the polarization of the photon. The polarization degree of the NLC photon is defined as

$$\Gamma(s_\gamma)=\frac{\mathrm{d}\mathsf{P}_\gamma^{\|}/\mathrm{d}s_\gamma-\mathrm{d}\mathsf{P}_\gamma^{\perp}/\mathrm{d}s_\gamma}{\mathrm{d}\mathsf{P}_\gamma/\mathrm{d}s_\gamma}, \tag{7}$$

where $\mathrm{d}\mathsf{P}_\gamma/\mathrm{d}s_\gamma=\mathrm{d}\mathsf{P}_\gamma^{\|}/\mathrm{d}s_\gamma+\mathrm{d}\mathsf{P}_\gamma^{\perp}/\mathrm{d}s_\gamma$. Following the definition in Eq. (7), we define the polarization degree for a distribution of photons to be Γ where $\Gamma=(\mathsf{P}_\gamma^{\|}-\mathsf{P}_\gamma^{\perp})/\mathsf{P}_\gamma$ and $\mathsf{P}_\gamma=\mathsf{P}_\gamma^{\|}-\mathsf{P}_\gamma^{\perp}$. For photons in the $\|$ polarization eigenstate, $\Gamma=1$; if they are in the $\perp$ eigenstate then $\Gamma=-1$ and if they are completely unpolarized, $\Gamma=0$.

A. Circularly polarized background

First, we investigate the potential harmonic structure in the energy spectrum of the outgoing positron. For the harmonic structure from both NLC and NBW steps to be discernible: (i) pairs must be produced by photons with momentum fractions around the first NLC harmonic $s_{\gamma,1}=2\eta/(2\eta+1+\xi^2)$; and (ii) the photon momentum fraction must be larger than the threshold for pair creation from a single laser photon, i.e. linear Breit Wheeler from the carrier frequency, which requires $2(1+\xi^2)/(\eta s_{\gamma,1})<1$. Combining these conditions, one arrives at the requirement on the initial electron's energy parameter of $\eta>(1+\sqrt{2})(1+\xi^2)$. For $\xi=1$, and a standard laser carrier frequency of 1.55 eV, this corresponds already to 407 GeV electrons (or an energy parameter of $\eta=4.83$). Therefore to demonstrate harmonic structure in the pair spectrum, we consider 500 GeV electrons colliding head-on with a 16 cycle, $\xi=1$ circularly polarized plane wave with carrier frequency 1.55 eV (i.e. $\eta=5.94$).

The double differential lightfront spectrum, $\mathrm{d}^2\mathsf{P}/\mathrm{d}s_q/\mathrm{d}s_\gamma$ for this case is plotted in Fig. 2(a). We see the main features: (i) the harmonic structures from the NLC spectrum are observed around the black dashed lines, namely $s_{\gamma,n}=2n\eta/(2n\eta+1+\xi^2)$ for $n=1$, 2. This is made manifest via the comparison with the red solid line which plots the NLC spectrum of photons before the pair is created; and (ii) the double differential spectrum rises up around the magenta dotted line, $s_q=\{1\pm[1-2(1+\xi^2)/(s_\gamma\eta)]^{1/2}\}/2$, corresponding to the edge of the first NBW harmonic triggered

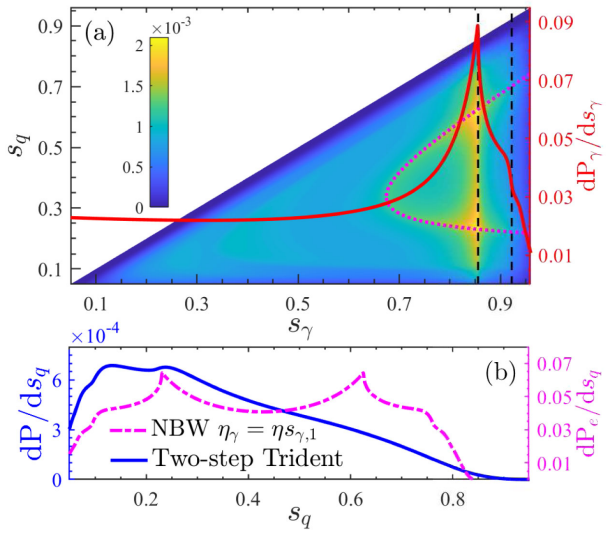

FIG. 2. Differential probability for the two-step trident process in a $\xi=1$, $N=16$, circularly polarized pulse of frequency 1.55 eV colliding head on with a 500 GeV electron, corresponding to an energy parameter of $\eta=5.94$. (a) Double lightfront spectrum, $\mathrm{d}^2\mathsf{P}/\mathrm{d}s_q/\mathrm{d}s_\gamma$ is plotted for the polarized intermediate photon and compared to the NLC spectrum (red overlaid line). The black dashed lines give the location of the first two harmonics in the photon spectrum at $s_{\gamma,n}=2n\eta/(2n\eta+1+\xi^2)$ for $n=1$, 2; the magenta dotted line denotes the location of the first harmonic in the positron spectrum created by the photon with the energy ηs_γ at $s_q=\{1\pm[1-2(1+\xi^2)/(s_\gamma\eta)]^{1/2}\}/2$. (b) Positron energy spectrum for the two-step trident process $\mathrm{dP}/\mathrm{d}s_q$ and for the NBW process $\mathrm{dP}_e/\mathrm{d}s_q$ created by the first-harmonic photon (with the energy parameter $\eta_\gamma=\eta s_{\gamma,1}$) in the NLC spectrum.

by the intermediate photon with the momentum fraction $s_\gamma>2(1+\xi^2)/\eta$. This is illustrated by the location of harmonic peaks in the NBW positron spectrum [magenta dot-dashed line plotted in Fig. 2(b)] created by a photon with energy equal to the edge of the first NLC harmonic range (the "Compton edge" [64]), with energy $\eta_\gamma=\eta s_{\gamma,1}$. The double differential spectrum peaks up around the crossing points between the first NLC-harmonic (black dashed) line and the first NBW-harmonic (magenta dotted) line in Fig. 2(a). After integrating over the photon lightfront momentum s_γ, the lower harmonic peak ($s_q=0.23$) remains in the positron spectrum of the nonlinear two-step trident process as shown in Fig. 2(b) (but the upper harmonic peak around $s_q=0.62$ is smoothed out.)

In Figs. 3(a) and 3(b), the double differential spectrum for a lower-energy case is plotted, in which an 80 GeV electron collides head-on with a 16 cycle circularly polarized plane wave pulse with carrier frequency at the third harmonic of the laser at 4.65 eV, corresponding to an energy parameter of $\eta=2.85$. In this case, harmonic structure is again present in the NLC photon spectrum (illustrated by the red solid line), but the energy parameter

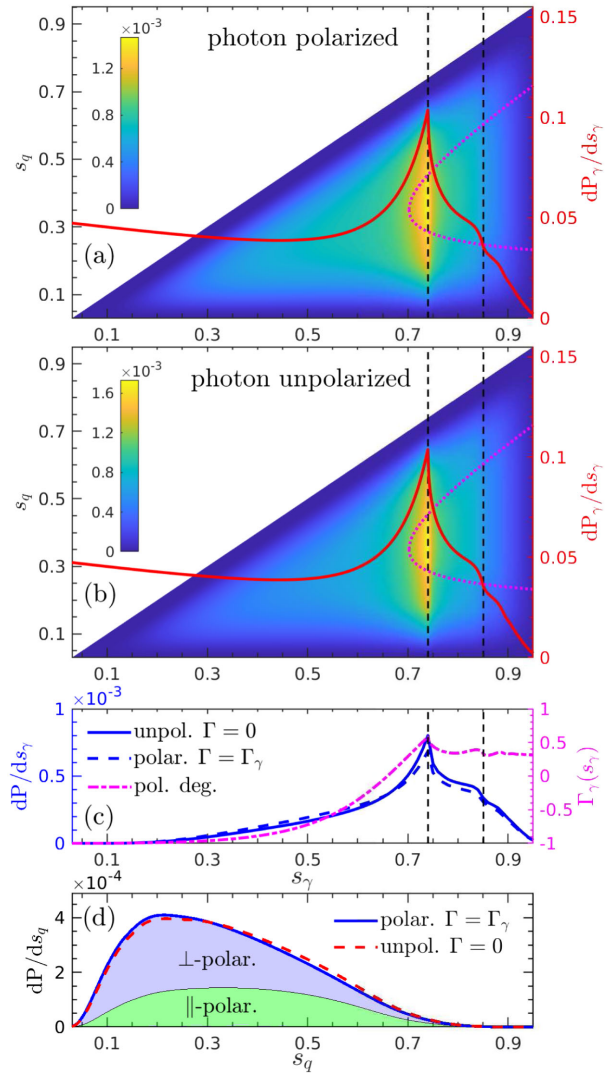

FIG. 3. Differential probability for the two-step trident process in a $\xi = 1$, $N = 16$, circularly polarized pulse of frequency 4.65 eV colliding head on with a 80 GeV electron, corresponding to an energy parameter of $\eta = 2.85$. The double lightfront spectra $\mathrm{d}^2\mathsf{P}/\mathrm{d}s_q/\mathrm{d}s_\gamma$ for the (a) polarized and (b) unpolarized photon and compared to the NLC spectrum (red overlaid line). The magenta dotted lines denote the location of the leading-NBW harmonic in the positron spectrum created by the photon with energy ηs_γ at $s_q = \{1 \pm [1 - 2(1+\xi^2)/(2s_\gamma\eta)]^{1/2}\}/2$. (c) Dependence of the probability on the lightfront momentum of a polarized (blue dashed line) and unpolarized (blue sold line) photon: for the polarized case, the polarization degree is given by the magenta dashed-dotted line. (d) Energy spectrum of the positron, $\mathrm{dP}/\mathrm{d}s_q$, for unpolarized ($\Gamma = 0$) and polarized ($\Gamma = \Gamma_\gamma$) intermediate photons. The shaded areas underneath the photon-polarized spectrum denote the contribution from each polarization eigenstate. In (a)–(c), the black dashed lines give the location of the first two harmonics in the photon spectrum at $s_\gamma = 2n\eta/(2n\eta + 1 + \xi^2)$ for $n = 1, 2$.

is significantly lower, $\eta < 2(1+\xi^2)$, so that pairs are only created via the nonlinear process, i.e. requiring higher harmonics from the laser. The leading NBW harmonic is now the second order with smooth harmonic edges, as shown in the figure by the magenta dotted line plotted at $s_q = \{1 \pm [1 - 2(1+\xi^2)/(2s_\gamma\eta)]^{1/2}\}/2$. Therefore, there is no noticeable NBW-harmonic structure remaining in the double differential spectrum of the trident process.

In Fig. 3(c), the single differential spectrum $\mathrm{dP}/\mathrm{d}s_\gamma$ is plotted, which shows the spectrum of photons that created pairs in the two-step trident process. The locations of the Compton harmonics can be clearly seen. We note that the major contribution originates from the middle of the s_γ-range. There is clearly a competition between: (i) more photons being produced at low values of s_γ, and (ii) pairs being created more easily for photons with higher values of s_γ. The optimum region of s_γ falls between these two extremes. For the parameters in Fig. 3, the low-order harmonics in the photon spectrum coincide with the optimal region, and therefore clear harmonic structures from the NLC spectrum can be observed in the double differential plots in Figs. 3(a) and 3(b). (As we will see later in Fig. 4, if the initial electron energy is lowered to 16.5 GeV, this optimal region of the photon spectrum corresponds to higher harmonic order and hence no harmonic structure is observable.) Despite the appearance of harmonic structure in the double differential for the 80 GeV electron case due to NLC, the harmonic structure is not passed on to the energy spectrum of the produced pair. This is because: (i) the Compton spectrum is integrated over, and (ii) pairs can only be created at higher harmonic order.

Now we consider the effect of photon polarization. For some parameters, the photon from NLC can be highly polarized [47,48], and since NBW can be strongly affected by the polarization of the photon [33,49,50,65], we expect photon polarization to play a role in the two-step trident process. The dependence of the differential probability on the polarization of the photon is plotted in Fig. 3. First, we see that the harmonic position in the double differential spectrum is unchanged when the photon is unpolarized in Fig. 3(b), which is to be expected, since polarization can only affect energy spectra of the photons in different states, but not the total photon spectrum and the kinematic ranges. However, in Fig. 3(c), we see that the *height* of the harmonic peak is reduced. This has a straightforward explanation when compared to the photon polarization degree at the harmonic peak. At this energy, photons are *more* likely to be produced by NLC in the $\parallel$ polarization state, which is the state *least* likely to produce pairs via NBW. This is why, for these parameters, including photon polarization leads to a suppression of pairs at the leading Compton harmonic. In general, we can see that photon polarization can have the affect of enhancing and suppressing different parts of the pair spectrum. For example in the same plot, we see that at photon energies lower than the first Compton harmonic, the spectrum of pairs is instead *enhanced*. Again, this can be understood by comparing

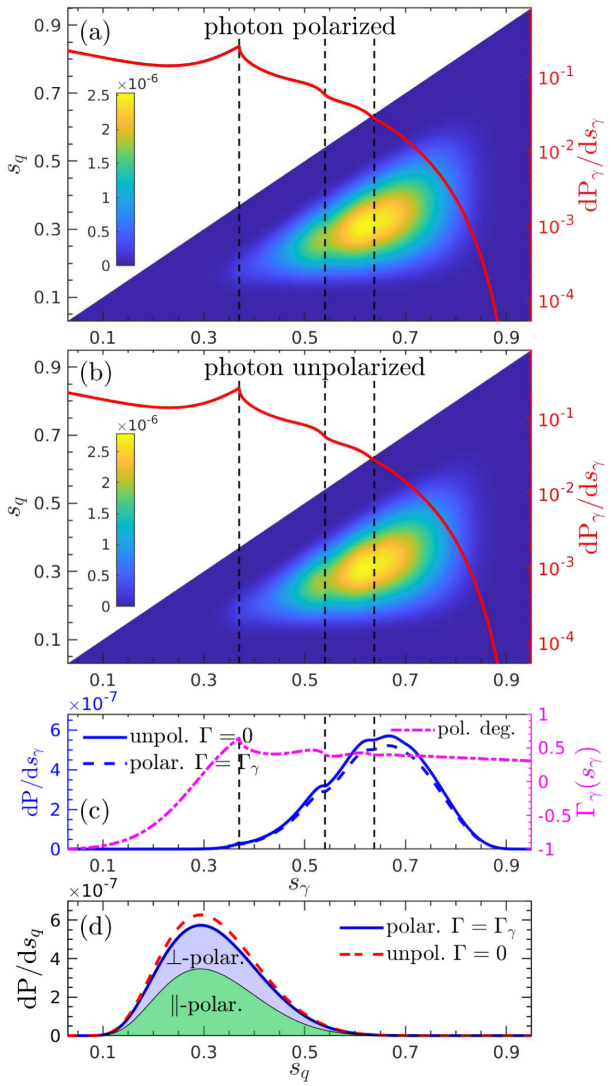

FIG. 4. Differential probability for the two-step trident process in a $\xi = 1$, $N = 16$, circularly polarized pulse of frequency 4.65 eV colliding head on with a 16.5 GeV electron, corresponding to an energy parameter of $\eta = 0.59$. The double lightfront spectra, $\mathrm{d}^2\mathrm{P}/\mathrm{d}s_q/\mathrm{d}s_\gamma$ are plotted for an (a) polarized and (b) unpolarized photons and compared to the NLC spectrum (red overlaid line). (c) The dependence of the probability on the lightfront momentum of a polarized (blue dashed line) and unpolarized (blue sold line) photon is plotted: for the polarized case, the polarization degree is given by the magenta dashed-dotted line. (d) The energy spectrum of the positron, $\mathrm{dP}/\mathrm{d}s_q$, for unpolarized ($\Gamma = 0$) and polarized ($\Gamma = \Gamma_\gamma$) intermediate photon is plotted. The shaded areas underneath the polarized spectrum denote the contributions from each polarization eigenstate. In (a)–(c), the black dashed lines give the location of the first three harmonics in the photon spectrum at $s_\gamma = 2n\eta/(2n\eta + 1 + \xi^2)$ for $n = 1, 2, 3$.

with the polarization degree, where we see that NLC is more likely to produce photons polarized in the $\perp$ polarization state, which is *more* likely to lead to NBW pair creation. While photon polarization can influence the pair spectrum, the total yield is not always affected: in Fig. 3(d) it can be seen that the integrals of the polarized and unpolarized spectra are approximately equal. However, for higher energies, e.g. those in Fig. 2, the yield can be increased due to photon polarization. In Fig. 2, because the first Compton harmonic appears at $s_{\gamma,1} \to 1$, the effect of the pair suppression due to the photon polarization in the regime $s_\gamma > s_{\gamma,1}$ can be weaker overall than the enhancement due to the photon polarization in the regime $s_\gamma < s_{\gamma,1}$. In contrast, for lower photon energies, as we will show in Fig. 4, the total trident yield can be noticeably reduced by photon polarization as only photons with $s_\gamma > s_{\gamma,1}$ can contribute effectively to the production process.

In Fig. 4, we present the results for a 16.5 GeV electron. For this lower energy, harmonic structures in the double differential lightfront spectrum are no longer observable because the main contribution is from higher-order harmonics (around $s_\gamma = 0.64$, the harmonic order is $n = 3$). The contribution from the most visible NLC harmonic at $n = 1$, is strongly suppressed. Also in this case, because of the photon polarization, the yield of pairs is slightly reduced around the central peak in the double-differential spectrum and because the contribution from photons at energies below the first NLC harmonic is so suppressed, the part of the spectrum where photon polarization *enhances* pair production is also suppressed. As a result, in Fig. 4(d), it can be seen that the integral of the polarized case is now noticeably smaller than the unpolarized case. The other notable difference from the high-energy case in Fig. 3 is that the photons polarized in the $\|$-eigenstate has larger contribution to the total positron yield from the NLC-polarized photons as shown in Fig. 4(d).

In Fig. 5 the total yield of positrons is calculated as a function of intensity for various photon polarization choices. With the increase of the laser intensity, the positron yield increases significantly. For single-vertex processes, it is known that as ξ increases, the LMA tends to the LCFA for a plane-wave background [40]. Since a locally constant field is the same for different circularly polarized background helicities, we expect that as ξ increases, the difference between each photon helicity state should decrease. This is indeed what we observe in the inset in Fig. 5. We also observe the converse: as ξ is reduced past $\xi = 1$, the relative importance of photon helicity increases. This is another example of physics that is beyond the locally constant-field approach. (The relative importance of the photon polarization with the change of the laser intensity for the two-step trident process will be discussed later in Fig. 8.)

B. Linearly polarized background

The LMA for a linearly polarized background is more computationally expensive to calculate than the LMA for a circularly polarized background due to the latter having azimuthal symmetry in the transverse plane. As a

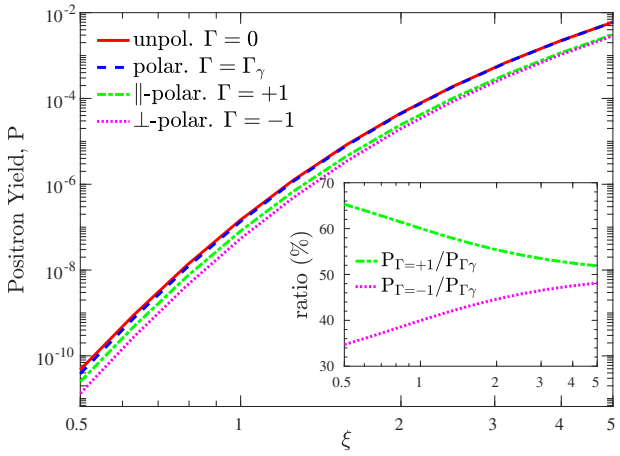

FIG. 5. Positron yield as a function of laser intensity for the two-step trident process in a head-on collision of a 16.5 GeV electron and a 16-cycle circularly polarized plane wave pulse with carrier frequency $\omega_l = 4.65$ eV (corresponding to $\eta = 0.59$). The plot shows the yield for photons that are unpolarized ($\Gamma = 0$), polarized by NLC ($\Gamma = \Gamma_\gamma$) or polarized in one of the eigenstates of the laser background ($\Gamma = \pm 1$). The inset shows the ratio of the yield for photons in a polarization eigenstate to the total yield for the NLC-polarized photons.

consequence, one must calculate generalized Bessel functions [32,66,67] in the integrand for a linearly polarized background, compared to just standard Bessel functions of the first kind for a circularly polarized background.

Here we perform a similar analysis as in the previous section but focus on the case of a 16.5 GeV electron colliding head-on with a $\xi = 1$, $N = 16$ *linearly* polarized pulse of frequency 4.65 eV, corresponding to an energy parameter of $\eta \approx 0.59$. In Fig. 6 rich harmonic structures are observed in the double differential plots, $\mathrm{d}^2\mathsf{P}/\mathrm{d}s_p/\mathrm{d}s_\gamma$ for a polarized [Fig. 6(a)] and unpolarized [Fig. 6(b)] intermediate photon. Again, these harmonic structures correspond to harmonics in the NLC spectrum and cannot be observed in the energy spectrum of the produced pair. Similar to the circularly polarized case, the effect of the photon polarization decreases the height of the harmonic peak in the double differential plots. However, in linearly polarized laser backgrounds, the photon is always more likely to be produced in the $\parallel$ polarization state ($\Gamma_\gamma > 0$), shown by the magenta line in Fig. 6(c). Therefore, even with very high-energy electrons, in a linearly polarized background, the effect of photon polarization is always to *reduce* the probability of nonlinear trident in the two-step process. Similar to the low-energy case in circularly polarized backgrounds, the photons in the $\parallel$-polarization eigenstate has a larger contribution to the total positron yield for the NLC-polarized photons in Fig. 6(d).

The positron yield is plotted against the background intensity parameter ξ in Fig. 7. As in the circularly polarized case, the positron yields for the unpolarized ($\Gamma = 0$) and polarized ($\Gamma = \Gamma_\gamma$) photon increase significantly with laser

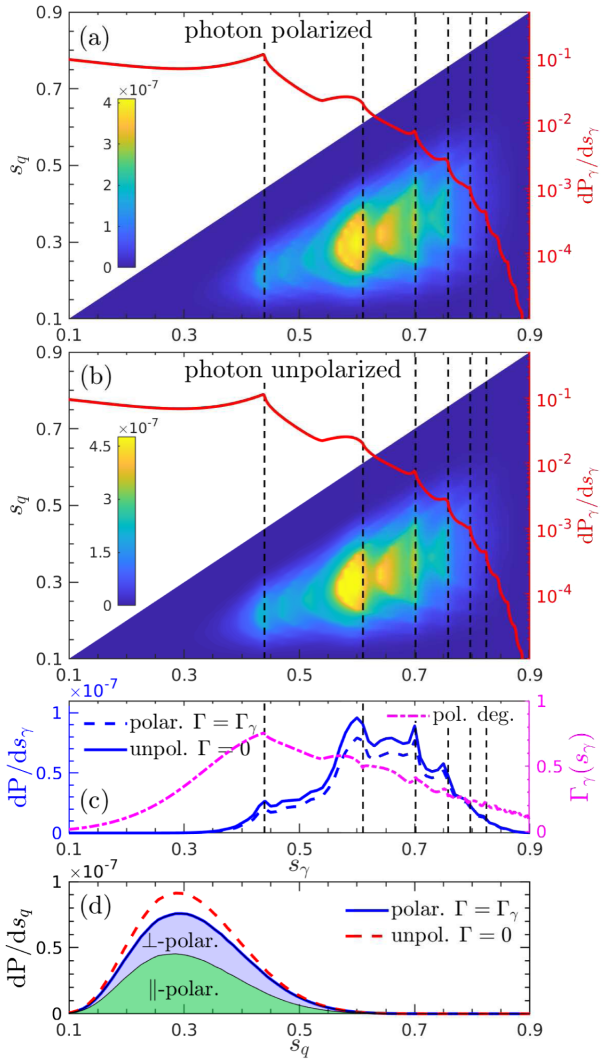

FIG. 6. Differential probability for the two-step trident process in a $\xi = 1$, $N = 16$, *linearly* polarized pulse of frequency 4.65 eV colliding head on with a 16.5 GeV electron, corresponding to an energy parameter of $\eta = 0.59$. The double lightfront spectra, $\mathrm{d}^2\mathrm{P}/\mathrm{d}s_q/\mathrm{d}s_\gamma$ are plotted for an (a) polarized and (b) unpolarized photon and compared to the NLC spectrum (red overlaid line). (c) Dependence of the probability on the lightfront momentum of a polarized (blue dashed line) and unpolarized (blue sold line) photon: for the polarized case, the polarization degree is given by the magenta dashed-dotted line. (d) Energy spectra of the positron, $\mathrm{dP}/\mathrm{d}s_q$ in the two-step trident process for the unpolarized ($\Gamma = 0$) and polarized ($\Gamma = \Gamma_\gamma$) photon. The shaded areas underneath the polarized spectrum denote the contributions from each polarization eigenstate. In (a)–(c), the black dashed lines give the location of the first six harmonics in the photon spectrum at $s_\gamma = 2n\eta/(2n\eta + 1 + \xi^2)$ for integers $n = 1$ to $n = 6$.

intensity, and in the photon-polarized case, the difference between the yield for each photon polarization eigenstate becomes smaller at higher intensities. However, in the linearly polarized background, the decrease of this difference is much slower than that in the circularly polarized

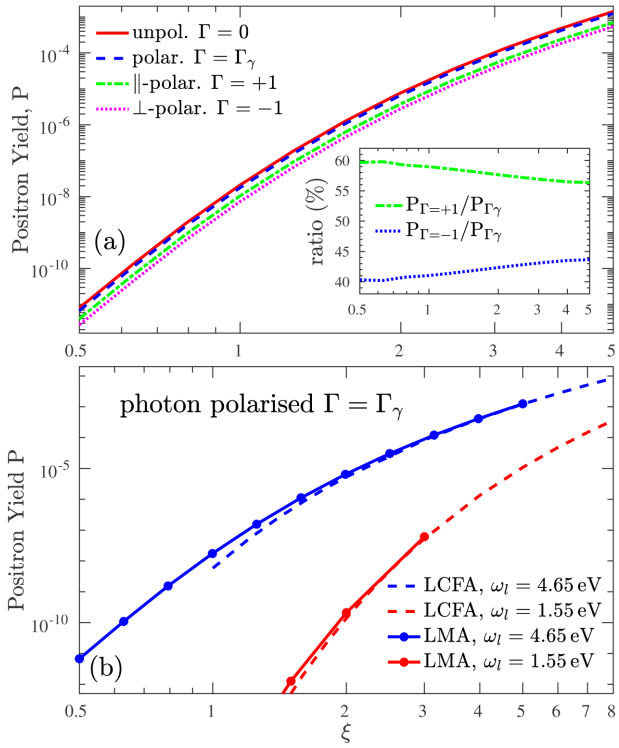

FIG. 7. Positron yield as a function of laser intensity for the two-step trident process in a head-on collision of a 16.5 GeV electron and a 16-cycle *linearly*-polarized plane wave pulse with carrier frequency $\omega = 4.65$ eV, corresponding to $\eta = 0.59$. In plot (a), the yield for photons that are unpolarized ($\Gamma = 0$), polarized by NLC ($\Gamma = \Gamma_\gamma$) or polarized in one of the eigenstates of the laser background ($\Gamma = \pm 1$) is shown; the inset shows the ratio of the yield for photons produced in a polarization eigenstate to the total yield for the NLC-polarized photons. In plot (b), the locally monochromatic approximation is compared to the locally constant field approximation for different laser carrier frequencies.

background, which implies that the polarization effects in linearly polarized backgrounds persist at much higher laser intensities (we will investigate this in the discussion in Sec. III). As the direction of polarization does not change with the phase in linearly polarized backgrounds, there is a well-defined constant field limit. In Fig. 7(b), the difference between the LMA and LCFA for predicting the positron yield is plotted. This illustrates the result that the LMA agrees with the LCFA at large intensity parameter ξ and at small intensities the LMA predicts higher positron yield than the LCFA. The threshold intensity for the agreement between the LMA and LCFA depends on the frequency of the background field: for the larger laser frequency, the LMA result matches the LCFA at higher intensities.

III. DISCUSSION

One of the motivations for the current work was to investigate harmonic structure in the two-step trident process. We found that the harmonic structure from the Compton step is generally washed out in the pair creation step, because the photon energies most likely to create pairs correspond to higher Breit-Wheeler harmonics where harmonic structure is no longer visible. The implications of this for n-step higher-order processes and cascades, is that harmonic structure from lower-order processes becomes washed out in later generations due to the light-front momentum being reduced. For a pair-creation stage, this is clear: to see harmonic structure requires the energy parameter to be of the order of $2(1+\xi^2)$; already for $\xi = 1$ and a triple-harmonic laser frequency of 4.65 eV this corresponds to around 130 GeV electrons. This washing-out of harmonic structure must also apply to multiple nonlinear Compton scattering of hard photons, where the Compton edge is at energy parameter $2\eta^2/(2\eta + 1 + \xi^2)$; as the energy parameter η reduces in each stage of the cascade, the Compton edge is pushed to lower energies, which are less likely to seed the next generation of the cascade. In order to obtain harmonic structures in later generations, which carry information of the subprocesses in earlier generations, the energy parameter needs to be very high. We demonstrated this for the two-step trident process by considering a 500 GeV electron in a circularly polarized background with frequency 1.55 eV.

Another motivation for the current work was to study the effect due to the intermediate photon being polarized. It is known from past studies of the trident process [17,27] that in a constant crossed field the relative importance of photon polarization is an order 10% effect. Indeed this is what we found using the LMA when the intensity parameter was increased toward the $\xi \gg 1$ region. However, with the LMA, we could also study the effect of photon polarization in the range when $\xi \gtrsim 1$, which is the parameter regime of some topical experiments E320 and LUXE that will employ electron beams from a linac.

In Fig. 8, we compare the relative importance of the polarization property of the intermediate photon in the two-step trident process in differently polarized laser backgrounds. In a *linearly*-polarized background, the effect of photon polarization in the two-step trident for likely future experimental parameters, is to *lower* the trident rate by around 15% in the intermediate intensity regime of $\xi \sim O(1)$. This agrees with a similar analysis performed for a constant crossed field background [27]. In a linearly polarized background, the direction of polarization does not change with phase in the lab frame, and therefore there is a well-defined constant field limit. However, for circular polarization, there is no well-defined constant-crossed field limit. Therefore, if the LCFA becomes more accurate as ξ is increased, the importance of photon polarization in circular backgrounds must reduce for larger ξ, which we indeed find in Fig. 8. For $\xi \lesssim 1$ in circular backgrounds, the polarization effect can also reduce the trident rate, in principle even more than 10%. Here we see the point of using the LMA,

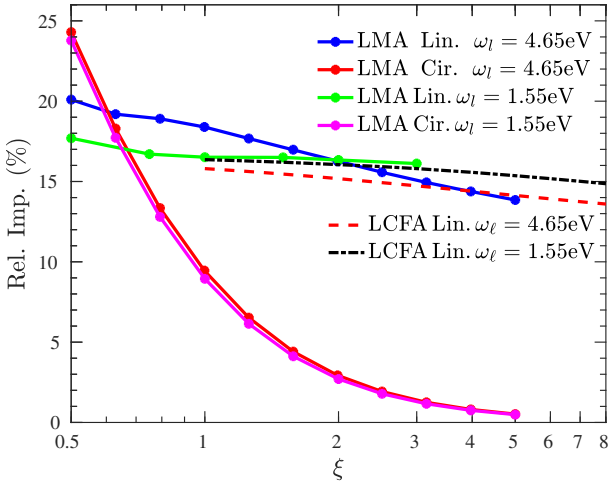

FIG. 8. The dependency on the intensity parameter of the "relative importance": $(P^{\Gamma=0} - P^{\Gamma=\Gamma_\gamma})/P^{\Gamma=\Gamma_\gamma}$ of the polarization of the intermediate photon in the two-step trident process is illustrated for differently polarized laser backgrounds. $N = 16$, $E_e = 16.5$ GeV.

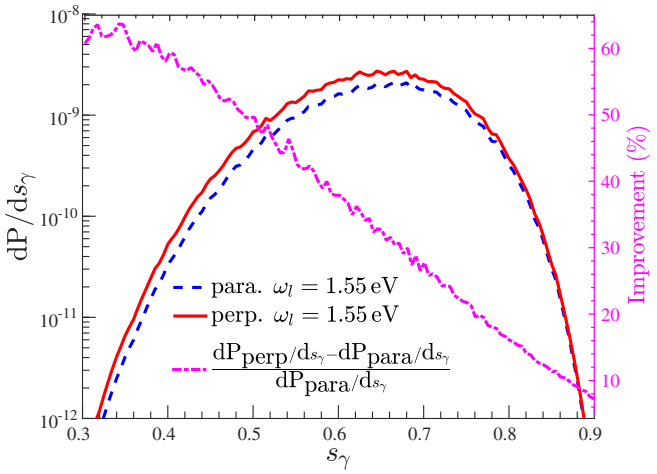

FIG. 9. Positron yield in the two-step trident scenario, in which a beam of 16.5 GeV electrons collide head-on with one plane-wave pulse to scatter highly polarized γ photons via nonlinear Compton scattering, which then collide with a second plane-wave pulse to create pairs via the nonlinear Breit-Wheeler process. Both the plane waves are 16-cycle linearly polarized pulses with intensity parameter $\xi = 2$ and carrier frequency 1.55 eV, which are polarized in the plane parallel or perpendicular to each other. The relative difference in the positron yield between the two cases is shown by the magenta line. P_{para} (P_{perp}) denotes the positron yield in the case with the parallel (perpendicular) polarization.

which has been used to calculate the polarization effect in the intermediate intensity region and in field backgrounds with the circular polarization. Agreement between the LMA and LCFA in the high-intensity region is shown in Fig. 8. Since the applicability of the LCFA also depends on the energy parameter, we include in the plot the leading and third harmonic of the background frequency. We see little difference in the relative importance although the energy parameter differs by a factor of three. This is perhaps due to the fact that, when all other parameters are fixed, for increasing energy parameter, the LCFA for NLC becomes *less* accurate, but the LCFA for NBW becomes *more* accurate. So while linear polarization is an attractive background to use for trident experiments since, for fixed laser pulse energy, it allows for ξ to be increased by a factor $\sqrt{2}$ compared to a circularly polarized background, we see that there is a slight cost to this increase when one takes into account the polarization of intermediate photons.

One may ask the question of whether knowledge of the influence of photon polarization can be used to optimize the two-step. Since nonlinear Compton most abundantly produces photons in the polarization state that is least likely to create pairs, if a single laser pulse is used, there is a natural compensation against the effects of polarization. However, if one uses a double laser pulse, with each subpulse being linearly polarized in a plane orthogonal to the polarization of the other pulse, and if one chooses the properties of the pulses such that in the first pulse mainly only nonlinear Compton scattering takes place, then one can engineer a situation in which the most abundantly produced polarization in nonlinear Compton scattering is also the polarization most likely to create pairs in the second pulse. Such an approach can be presumably generalized to n-stage processes, depending on which subprocess is favored in each generation.

The total yield of pairs in this two-step scenario can be calculated as in the previous sections using Eq. (2), but now where the corresponding phase integrals for NLC and NBW correspond to an integral over different laser pulses. In Fig. 9, we compare the positron yield in the double laser pulses with the parallel and perpendicular linear polarization. As we can see, by using laser pulses with orthogonal polarizations, one can improve the positron yield about 32% than that from the two laser pulses with the parallel polarization.

IV. CONCLUSION

In the two-step trident process, photon polarization can have an O(10%) effect on the total rate. This conclusion agrees with previous studies in a constant crossed field and via the locally constant field approximation, which one would expect to be a good approximation when $\xi \gg 1$. What is new here is that we have used the locally monochromatic approximation, which allowed us to analyze $\xi \sim O(1)$ as well as backgrounds with circularly polarization. We find that the effect of photon polarization increases slightly for a linearly polarized background as ξ is made smaller; for a circularly polarized background, photon polarization is only $O(10\%)$ for $\xi \lesssim 1$: as ξ is increased above this, the effect of photon polarization disappears. In order to reach this conclusion we have

derived photon-polarized rates for nonlinear Compton scattering and nonlinear Breit-Wheeler pair creation, in both a circularly polarized and a linearly polarized background. Such expressions can be useful in extending simulation codes based on the locally monochromatic approximation to include photon-polarized subprocesses.

If the energy of the scattered electrons and positrons were measured in experiment, the double-differential probability can in principle show harmonic structure from the Compton step intersecting with harmonic structure from nonlinear Breit-Wheeler. However, this can only be achieved if the centre-of-mass energy for a single background photon colliding with the electron is significantly over the threshold for linear Breit-Wheeler. We illustrated this with an example of 500 GeV electrons and a 1.55 eV laser frequency. In general we conclude that harmonic structure will be washed out in later generations in any n-step process such as a QED cascade.

Finally, one way to exploit the dependence on photon polarization to enhance the two-step trident process, is to collide initial electrons with two linearly polarized laser pulses, which have perpendicular polarizations. This can lead to an enhancement of around 30% compared to two pulses with the same polarization.

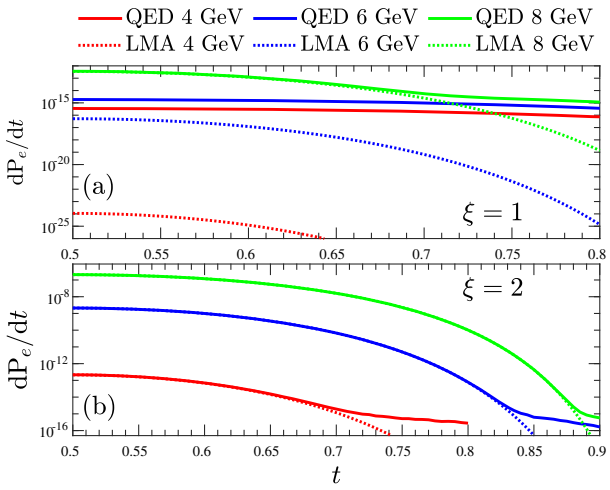

FIG. 10. Benchmark of the LMA positron spectra $\mathrm{d}P_e/\mathrm{d}t$ with the full QED calculations for the nonlinear Breit-Wheeler pair production in a circularly polarized laser background for different photon energies. The laser pulse has the carrier frequency $\omega_l = 1.55$ eV, 16 cycles and an amplitude of (a) $\xi = 1$; and (b) $\xi = 2$. The fraction of the lightfront momentum taken by the positron from the incident photon is denoted in this section only, by s_q.

ACKNOWLEDGMENTS

S. T. acknowledges support from the Shandong Provincial Natural Science Foundation, Grant No. ZR202102280476. B. K. acknowledges the hospitality of the DESY theory group and support from the Deutsche Forschungsgemeinschaft (DFG, German Research Foundation) under Germany's Excellence Strategy—EXC 2121 "Quantum Universe"—390833306. The work was carried out at Marine Big Data Center of Institute for Advanced Ocean Study of Ocean University of China.

APPENDIX A: BANDWIDTH EFFECT AT LOWER ELECTRON ENERGIES

As mentioned in the Introduction, when the initial electron energy parameter η is sufficiently low, bandwidth effects become important in the process of pair creation, and therefore also in the trident process. If the strong-field parameter $\chi = \eta\xi$ satisfies $\chi \ll 1$, pair-creation is strongly suppressed. This suppression can be partially reduced due to the contribution from linear Breit-Wheeler using photons from the upper half of the bandwidth of the pulse (see e.g. [68,69] where this effect was first reported, for more details on this point). Essentially, there are two routes to pair-creation: (i) via nonlinear Breit-Wheeler with the background photons with energies at the carrier frequency; and (ii) via linear Breit-Wheeler with high energy background photons from the upper wings of the pulse bandwidth (they are suppressed, since they are in the wings). For $\chi \sim O(1)$, nonlinear Breit-Wheeler is dominant for the parameters studied in this paper. As χ is reduced and enters the $\chi < 1$ region, eventually, nonlinear Breit-Wheeler is suppressed exponentially and for small enough χ, it is suppressed even more than the linear Breit-Wheeler contribution, which can become dominant. This is an artefact due to the theoretical description of the pulse (in reality, such high energy photons from the pulse would not be transmitted through all the optical elements of an experiment). This bandwidth effect was also recently studied in relation to the LMA for Breit-Wheeler [41,53] and also nonlinear Compton scattering [42,52].

In relation to the trident process, the finite bandwidth of the pulse mostly affects the nonlinear Breit-Wheeler step. In Fig. 10, we compare the positron lightfront momentum spectra $\mathrm{d}P_e/\mathrm{d}t$ acquired from the full QED expression and the LMA calculations, where we recall that t is the fraction of the lightfront momentum taken by the positron from the incident photon. We see that, as the photon energy is reduced, the LMA becomes increasingly inaccurate. To interpret the accuracy for predicting the two-step trident process, one needs to take into account that the photon energy emitted in the first step that is most likely to create pairs, is at around half of the electron energy (for the parameters studied in this paper, it is at around 60% of the electron energy). Therefore if $\xi = 1$ and the LMA starts to become inaccurate for, say 8 GeV photons for the NBW process, this means that the LMA for the two-step trident will likely become inaccurate for an initial electron energy lower than 16 GeV (for the specific parameters used here, we estimate this to be around 13.3 GeV). This cutoff energy, below which benchmarking the LMA with the full

QED expression loses its applicability, depends on χ; if ξ and η (or ω_l) were increased, the cutoff energy would be lower as can be seen from Fig. 10.

We emphasize that this discrepancy between the full QED and the LMA approach is a theoretical artefact and would not be an issue in a real experiment. Even if an experiment were deliberately made to transmit the high-frequency components of the laser pulse, the region where the LMA becomes inaccurate corresponds to very few pairs being created, and so is practically experimentally inaccessible.

APPENDIX B: LMA FORMULAS FOR POLARIZED NONLINEAR COMPTON AND BREIT-WHEELER

All LMA probabilities, P, can be written as a sum over partial probabilities, P_n, corresponding to integer harmonics n, with the lower bound of the sum $\lceil n^* \rceil$ depending on the process and experimental parameters. The total probability is calculated as an integral over the lightfront spectrum $\mathrm{d}\mathsf{P}/\mathrm{d}s = \sum_{n=\lceil n^*(s)\rceil}^{\infty} \mathrm{d}\mathsf{P}_n/\mathrm{d}s$ of one of the outgoing particles.

The photon polarization eigenstates are defined as:

$$\epsilon^\mu_{1,2} = \epsilon^\mu_{1,2} - \frac{\ell\cdot\epsilon_{1,2}}{k\cdot\ell}k^\mu; \qquad \varepsilon^\mu_{\pm} = \epsilon^\mu_{\pm} - \frac{\ell\cdot\epsilon_{\pm}}{k\cdot\ell}k^\mu, \tag{B1}$$

where $\epsilon_\pm = (\epsilon_1 \pm i\epsilon_2)/\sqrt{2}$ and $\epsilon^\mu_j = \delta^\mu_j$. where $\varepsilon^\mu_{1,2}$ are the eigenstates in a linearly polarized plane wave background and $\varepsilon^\mu_\pm$ those in a circularly polarized plane-wave background. The designation: $\parallel$ ($\perp$) refers to ε_1 (ε_2) in a linearly polarized background and in a circularly polarized background to photons polarized in the ε_+ (ε_-) state, which are states with the opposite (same) helicity as the background.

The photon polarization degree of the photons, can be defined for the entire spectrum, Γ; for a particular photon energy in the spectrum $\Gamma(s)$; or for a particular photon energy at a given instantaneous value of the phase, ϕ as $\Gamma(s,\phi)$. Explicitly, the definitions are

$$\Gamma = \frac{\mathsf{P}^\parallel - \mathsf{P}^\perp}{\mathsf{P}^\parallel + \mathsf{P}^\perp}; \qquad \Gamma(s) = \frac{\mathrm{d}\mathsf{P}^\parallel(s)/\mathrm{d}s - \mathrm{d}\mathsf{P}^\perp(s)/\mathrm{d}s}{\mathrm{d}\mathsf{P}^\parallel(s)/\mathrm{d}s + \mathrm{d}\mathsf{P}^\perp(s)/\mathrm{d}s};$$
$$\Gamma(s,\phi) = \frac{\mathrm{d}^2\mathsf{P}^\parallel(s,\phi)/\mathrm{d}s\mathrm{d}\phi - \mathrm{d}^2\mathsf{P}^\perp(s,\phi)/\mathrm{d}s\mathrm{d}\phi}{\mathrm{d}^2\mathsf{P}^\parallel(s,\phi)/\mathrm{d}s\mathrm{d}\phi + \mathrm{d}^2\mathsf{P}^\perp(s,\phi)/\mathrm{d}s\mathrm{d}\phi}. \tag{B2}$$

These relations can be straightforwardly inverted, e.g. $\mathsf{P}^\parallel = \mathsf{P}(1+\Gamma)/2$, and $\mathsf{P}^\perp = \mathsf{P}(1-\Gamma)/2$.

First-order rates are usually defined in terms of the lightfront momentum fraction $s \in [0,1]$ of the incoming particle. For the two-step trident process, in the NBW part, the lightfront momentum fraction of the positron s_q is not bounded by 1, but instead, $s_q \in [0, s_\gamma]$, as explained in Eq. (4). Therefore, to keep these definitions as referring to single-vertex processes, we introduce the lightfront momentum variable for the positron $t = s_q/s_\gamma$, so that $t \in [0,1]$.

1. Photon-polarized nonlinear Compton scattering in a circularly polarized background

The partial lightfront momentum spectrum, $\mathrm{d}\mathsf{P}^{\parallel(\perp)}_{\mathsf{cp},\gamma,n}/\mathrm{d}s$, of photons in the $\parallel(\perp)$-state emitted by an unpolarized electron with energy parameter η via nonlinear Compton scattering in a circularly polarized plane wave background is given by:

$$\frac{\mathrm{d}\mathsf{P}^{\parallel}_{\mathsf{cp},\gamma,n}}{\mathrm{d}s} = \frac{\alpha}{2\eta}\int \mathrm{d}\phi\Theta[n - n^*_{\mathsf{cp},\gamma}(\phi)]\Big\{\xi^2(\phi)\Big[J'^2_n(z_{\gamma,n}) + \frac{n^2}{(z_{\gamma,n})^2}J^2_n(z_{\gamma,n}) - J^2_n(z_{\gamma,n})\Big]h_s - J^2_n(z_{\gamma,n}) + 2h_s\frac{\xi(\phi)}{\mathcal{P}_{\mathsf{cp},\gamma,n}}\left(1+\xi^2(\phi) - n\eta\frac{1-s}{s}\right) \times J'_n(z_{\gamma,n})J_n(z_{\gamma,n})\Big\}, \tag{B3a}$$

$$\frac{\mathrm{d}\mathsf{P}^{\perp}_{\mathsf{cp},\gamma,n}}{\mathrm{d}s} = \frac{\alpha}{2\eta}\int \mathrm{d}\phi\Theta[n - n^*_{\mathsf{cp},\gamma}(\phi)]\Big\{\xi^2(\phi)\Big[J'^2_n(z_{\gamma,n}) + \frac{n^2}{(z_{\gamma,n})^2}J^2_n(z_{\gamma,n}) - J^2_n(z_{\gamma,n})\Big]h_s - J^2_n(z_{\gamma,n}) - 2h_s\frac{\xi(\phi)}{\mathcal{P}_{\mathsf{cp},\gamma,n}}\left(1+\xi^2(\phi) - n\eta\frac{1-s}{s}\right) \times J'_n(z_{\gamma,n})J_n(z_{\gamma,n})\Big\}, \tag{B3b}$$

where $\xi(\phi) \equiv \xi f(\phi)$, and

$$z_{\gamma,n} = \frac{s\xi(\phi)}{\eta(1-s)}\mathcal{P}_{\mathsf{cp},\gamma,n}, \quad \mathcal{P}_{\mathsf{cp},\gamma,n} = \sqrt{2n\eta\frac{1-s}{s} - 1 - \xi^2(\phi)},$$
$$n^{\mathsf{cp}}_{*,\gamma}(\phi) = \frac{s[1+\xi^2(\phi)]}{2\eta(1-s)}, \quad h_s = \frac{1+(1-s)^2}{2(1-s)}.$$

The total spectrum of the emitted photon from an unpolarized electron in a circularly polarized background can then be given as

$$\frac{\mathrm{d}}{\mathrm{d}s}\mathsf{P}_{\mathsf{cp},\gamma,n} = \frac{\mathrm{d}}{\mathrm{d}s}\mathsf{P}^{\parallel}_{\mathsf{cp},\gamma,n} + \frac{\mathrm{d}}{\mathrm{d}s}\mathsf{P}^{\perp}_{\mathsf{cp},\gamma,n}.$$

2. Photon-polarized nonlinear Breit-Wheeler pair-creation in a circularly polarized background

The partial lightfront momentum spectrum, $\mathrm{d}\mathsf{P}^{\parallel(\perp)}_{\mathsf{cp},e,n}/\mathrm{d}t$ of positrons created via the nonlinear Breit-Wheeler process in a circularly polarized plane wave background by a

photon with energy parameter η_ℓ and polarized in the $\parallel(\perp)$-eigenstate is given by:

$$\frac{\mathrm{d}\mathsf{P}^{\parallel}_{\mathsf{cp},e,n}}{\mathrm{d}t} = \frac{\alpha}{\eta_\ell}\int \mathrm{d}\varphi\Theta[n-n^*_{\mathsf{cp},e}(\phi)]\Big\{J_n^2(z_{e,n})+\xi^2(\phi) \times\left[\frac{n^2}{(z_{e,n})^2}J_n^2(z_{e,n})+J'^2_n(z_{e,n})-J_n^2(z_{e,n})\right]g_t +\frac{2\xi(\phi)}{\mathcal{P}_{\mathsf{cp},e,n}}[n\eta_\ell t(1-t)-1-\xi^2(\phi)]J'_n(z_{e,n}) \times J_n(z_{e,n})g_t\Big\}, \tag{B4a}$$

$$\frac{\mathrm{d}\mathsf{P}^{\perp}_{\mathsf{cp},e,n}}{\mathrm{d}t} = \frac{\alpha}{\eta_\ell}\int \mathrm{d}\varphi\Theta[n-n^*_{\mathsf{cp},e}(\phi)]\Big\{J_n^2(z_{e,n})+\xi^2(\phi) \times\left[\frac{n^2}{(z_{e,n})^2}J_n^2(z_{e,n})+J'^2_n(z_{e,n})-J_n^2(z_{e,n})\right]g_t -\frac{2\xi(\phi)}{\mathcal{P}_{\mathsf{cp},e,n}}[n\eta_\ell t(1-t)-1-\xi^2(\phi)]J'_n(z_{e,n}) \times J_n(z_{e,n})g_t\Big\}, \tag{B4b}$$

where

$$z_{e,n}=\frac{\xi(\phi)\mathcal{P}_{\mathsf{cp},e,n}}{\eta_\ell t(1-t)},\ \mathcal{P}_{\mathsf{cp},e,n}=\sqrt{2n\eta_\ell t(1-t)-1-\xi^2(\phi)},$$
$$n^*_{\mathsf{cp},e}(\phi)=\frac{1+\xi^2(\phi)}{2\eta_\ell t(1-t)},\ g_t=\frac{t^2+(1-t)^2}{2t(1-t)}.$$

We can then obtain the positron lightfront spectrum created by an unpolarized photon in a circularly polarized background as

$$\frac{\mathrm{d}}{\mathrm{d}t}\mathsf{P}_{\mathsf{cp},e,n}=\frac{1}{2}\left(\frac{\mathrm{d}}{\mathrm{d}t}\mathsf{P}^{\parallel}_{\mathsf{cp},e,n}+\frac{\mathrm{d}}{\mathrm{d}t}\mathsf{P}^{\perp}_{\mathsf{cp},e,n}\right).$$

3. Photon-polarized nonlinear Compton scattering in a linearly polarized background

The partial lightfront spectrum, $\mathrm{d}\mathsf{P}^{\parallel(\perp)}_{\mathsf{lp},\gamma,n}/\mathrm{d}s$, of photons in the $\parallel(\perp)$-state emitted by an unpolarized electron with energy parameter η via nonlinear Compton scattering in a linearly polarized plane wave background is given by:

$$\frac{\mathrm{d}\mathsf{P}^{\parallel}_{\mathsf{lp},\gamma,n}}{\mathrm{d}s}=\frac{\alpha}{2\eta}\int \mathrm{d}\phi\Theta[n-n^*_{\mathsf{lp},\gamma}(\phi)]\int_{-\pi}^{\pi}\frac{\mathrm{d}\theta}{2\pi}\{\xi^2(\phi)[\Lambda^2_{1,n}(\alpha_\gamma,\beta_\gamma) -\Lambda_{0,n}(\alpha_\gamma,\beta_\gamma)\Lambda_{2,n}(\alpha_\gamma,\beta_\gamma)]h_s-\Lambda^2_{0,n}(\alpha_\gamma,\beta_\gamma) +[\Lambda_{0,n}(\alpha_\gamma,\beta_\gamma)\mathcal{P}_{\mathsf{lp},\gamma,n}\cos\theta-\xi(\phi)\Lambda_{1,n}(\alpha_\gamma,\beta_\gamma)]^2 -[\Lambda_{0,n}(\alpha_\gamma,\beta_\gamma)\mathcal{P}_{\mathsf{lp},\gamma,n}\sin\theta]^2\}, \tag{B5a}$$

$$\frac{\mathrm{d}\mathsf{P}^{\perp}_{\mathsf{lp},\gamma,n}}{\mathrm{d}s}=\frac{\alpha}{2\eta}\int \mathrm{d}\phi\Theta[n-n^*_{\mathsf{lp},\gamma}(\phi)]\int_{-\pi}^{\pi}\frac{\mathrm{d}\theta}{2\pi}\{\xi^2(\phi)[\Lambda^2_{1,n}(\alpha_\gamma,\beta_\gamma) -\Lambda_{0,n}(\alpha_\gamma,\beta_\gamma)\Lambda_{2,n}(\alpha_\gamma,\beta_\gamma)]h_s-\Lambda^2_{0,n}(\alpha_\gamma,\beta_\gamma) -[\Lambda_{0,n}(\alpha_\gamma,\beta_\gamma)\mathcal{P}_{\mathsf{lp},\gamma,n}\cos\theta-\xi(\phi)\Lambda_{1,n}(\alpha_\gamma,\beta_\gamma)]^2 +[\Lambda_{0,n}(\alpha_\gamma,\beta_\gamma)\mathcal{P}_{\mathsf{lp},\gamma,n}\sin\theta]^2\}, \tag{B5b}$$

where

$$\mathcal{P}_{\mathsf{lp},\gamma,n}=\sqrt{2n\eta\frac{1-s}{s}-1-\frac{1}{2}\xi^2(\phi)},$$
$$n^*_{\mathsf{lp},\gamma}(\phi)=\frac{s[1+\xi^2(\phi)/2]}{2\eta(1-s)},\qquad \alpha_\gamma=\mathcal{P}_{\mathsf{lp},\gamma,n}\frac{s\xi(\phi)\cos\theta}{\eta(1-s)},$$
$$\beta_\gamma=\frac{s\xi^2(\phi)}{8\eta(1-s)}.$$

and

$$\Lambda_{0,n}(x,y)=\sum_{k=-\infty}^{\infty}J_{n+2k}(x)J_k(y), \tag{B6a}$$
$$\Lambda_{1,n}(x,y)=\frac{1}{x}\sum_{k=-\infty}^{\infty}(n+2k)J_{n+2k}(x)J_k(y) \tag{B6b}$$
$$\Lambda_{2,n}(x,y)=\frac{1}{2}\sum_{k=-\infty}^{\infty}J_{n+2k}(x)\left(\frac{k}{y}+1\right)J_k(y), \tag{B6c}$$

The total spectrum of the emitted photon from an unpolarized electron can then be given as

$$\frac{\mathrm{d}\mathsf{P}_{\mathsf{lp},\gamma,n}}{\mathrm{d}s}=\frac{\mathrm{d}\mathsf{P}^{\parallel}_{\mathsf{lp},\gamma,n}}{\mathrm{d}s}+\frac{\mathrm{d}\mathsf{P}^{\perp}_{\mathsf{lp},\gamma,n}}{\mathrm{d}s}.$$

4. Photon-polarized nonlinear Breit-Wheeler pair-creation in a linearly polarized background

The partial lightfront momentum spectrum, $\mathrm{d}\mathsf{P}^{\parallel(\perp)}_{\mathsf{lp},e,n}/\mathrm{d}t$ of positrons created via the nonlinear Breit-Wheeler process in a linearly polarized plane wave background by a photon with energy parameter η_ℓ and polarized in the $\parallel(\perp)$-state is given by:

$$\frac{\mathrm{d}\mathsf{P}^{\parallel}_{\mathsf{lp},e,n}}{\mathrm{d}t}=\frac{\alpha}{\eta_\ell}\int \mathrm{d}\phi\Theta[n-n^*_{\mathsf{lp},e}(\phi)]\int_{-\pi}^{\pi}\frac{\mathrm{d}\theta}{2\pi}\{\xi^2(\phi)[\Lambda^2_{1,n}(\alpha_e,\beta_e) -\Lambda_{0,n}(\alpha_e,\beta_e)\Lambda_{2,n}(\alpha_e,\beta_e)]g_t+\Lambda^2_{0,n}(\alpha_e,\beta_e) +[\Lambda_{0,n}(\alpha_e,\beta_e)\mathcal{P}_{\mathsf{lp},e,n}\sin\theta]^2-[\Lambda_{0,n}(\alpha_e,\beta_e) \times\mathcal{P}_{\mathsf{lp},e,n}\cos\theta-\xi(\phi)\Lambda_{1,n}(\alpha_e,\beta_e)]^2\}, \tag{B7a}$$

$$\frac{\mathrm{d}\mathsf{P}^{\perp}_{\mathsf{lp},e,n}}{\mathrm{d}t}=\frac{\alpha}{\eta_\ell}\int \mathrm{d}\phi\Theta[n-n^*_{\mathsf{lp},e}(\phi)]\int_{-\pi}^{\pi}\frac{\mathrm{d}\theta}{2\pi}\{\xi^2(\phi)[\Lambda^2_{1,n}(\alpha_e,\beta_e) -\Lambda_{0,n}(\alpha_e,\beta_e)\Lambda_{2,n}(\alpha_e,\beta_e)]g_t+\Lambda^2_{0,n}(\alpha_e,\beta_e) -[\Lambda_{0,n}(\alpha_e,\beta_e)\mathcal{P}_{\mathsf{lp},e,n}\sin\theta]^2+[\Lambda_{0,n}(\alpha_e,\beta_e) \times\mathcal{P}_{\mathsf{lp},e,n}\cos\theta-\xi(\phi)\Lambda_{1,n}(\alpha_e,\beta_e)]^2\}, \tag{B7b}$$

where the expressions of $\Lambda_{j,n}$ for $j \in \{0,1,2\}$ are the same as in Eq. (B6), and

$$\mathcal{P}_{\mathsf{lp},e,n} = \sqrt{2n\eta_\ell t(1-t) - 1 - \frac{1}{2}\xi^2(\phi)},$$
$$n^*_{\mathsf{lp},e}(\phi) = \frac{1+\xi^2(\phi)/2}{2\eta_\ell t(1-t)}, \qquad \alpha_e = \mathcal{P}_{\mathsf{lp},e,n}\frac{\xi(\phi)\cos\theta}{\eta_\ell(1-t)t},$$
$$\beta_e = \frac{\xi^2(\phi)}{8t\eta_\ell(1-t)}.$$

The partial lightfront momentum spectrum of the positrons created by an unpolarized photon in a linearly polarized plane wave background is then given by

$$\frac{\mathrm{d}\mathsf{P}_{\mathsf{lp},e,n}}{\mathrm{d}t} = \frac{1}{2}\left(\frac{\mathrm{d}\mathsf{P}^{\parallel}_{\mathsf{lp},e,n}}{\mathrm{d}t} + \frac{\mathrm{d}\mathsf{P}^{\perp}_{\mathsf{lp},e,n}}{\mathrm{d}t}\right).$$

APPENDIX C: TABLE OF COMMON PARAMETERS

Below is a table of common parameters used in the manuscript.

TABLE I. Common parameters used in analysis. The detailed definition of each parameter is given in the main text.

ξ	Dimensionless laser intensity
η	Dimensionless energy parameter
N	Number of laser pulse cycles
$\phi = \varkappa \cdot x$	Laser phase
s_q	Lightfront momentum fraction of created positron
s_γ	Lightfront momentum fraction of NLC photon
Γ_γ	Polarization degree of the NLC photon
P	Total probability for the two-step trident
P_γ	Probability for the NLC-step
P_e	Probability for the NBW-step

[1] C. Bula *et al.* (E144 Collaboration), Phys. Rev. Lett. **76**, 3116 (1996).
[2] D. L. Burke *et al.*, Phys. Rev. Lett. **79**, 1626 (1997).
[3] C. Bamber *et al.*, Phys. Rev. D **60**, 092004 (1999).
[4] C. F. Nielsen, R. Holtzapple, M. M. Lund, J. H. Surrow, A. H. Sørensen, and U. I. Uggerhøj, Phys. Rev. Lett. **130**, 071601 (2023).
[5] Z. Chen, S. Meuren, E. Gerstmayr, V. Yakimenko, P. H. Bucksbaum, and D. A. Reis, Preparation of Strong-field QED Experiments at FACET-II, in *Optica High-brightness Sources and Light-Driven Interactions Congress 2022* (Optica Publishing Group, 2022), p. HF4B.6.
[6] H. Abramowicz *et al.*, Eur. Phys. J. Spec. Top. **230**, 2445 (2021).
[7] H. Hu, C. Müller, and C. H. Keitel, Phys. Rev. Lett. **105**, 080401 (2010).
[8] A. Ilderton, Phys. Rev. Lett. **106**, 020404 (2011).
[9] H. Hu and J. Huang, Phys. Rev. A **89**, 033411 (2014).
[10] V. Dinu and G. Torgrimsson, Phys. Rev. D **97**, 036021 (2018).
[11] F. Mackenroth and A. Di Piazza, Phys. Rev. D **98**, 116002 (2018).
[12] V. Dinu and G. Torgrimsson, Phys. Rev. D **101**, 056017 (2020).
[13] G. Torgrimsson, Phys. Rev. D **107**, 016019 (2023).
[14] V. N. Baier, V. M. Katkov, and V. M. Strakhovenko, Sov. Phys. Nucl. Phys. **14**, 572 (1972).
[15] V. I. Ritus, Nucl. Phys. **B44**, 236 (1972).
[16] D. A. Morozov and N. B. Narozhnyi, Zh. Eksp. Teor. Fiz. **30**, 44 (1977).
[17] B. King and H. Ruhl, Phys. Rev. D **88**, 013005 (2013).
[18] B. King and A. M. Fedotov, Phys. Rev. D **98**, 016005 (2018).
[19] O. P. Novak and R. I. Kholodov, Phys. Rev. D **86**, 105013 (2012).
[20] G. Torgrimsson, Phys. Rev. D **102**, 096008 (2020).
[21] A. I. Titov, U. H. Acosta, and B. Kampfer, Phys. Rev. A **104**, 062811 (2021).
[22] J. Z. Kamiński and K. Krajewska, arXiv:2211.04716.
[23] J. M. Cole, K. T. Behm, E. Gerstmayr, T. G. Blackburn, J. C. Wood, C. D. Baird, M. J. Duff, C. Harvey, A. Ilderton, A. S. Joglekar *et al.*, Phys. Rev. X **8**, 011020 (2018).
[24] K. Poder, M. Tamburini, G. Sarri, A. Di Piazza, S. Kuschel, C. D. Baird, K. Behm, S. Bohlen, J. M. Cole, D. J. Corvan *et al.*, Phys. Rev. X **8**, 031004 (2018).
[25] A. Di Piazza, T. N. Wistisen, M. Tamburini, and U. I. Uggerhøj, Phys. Rev. Lett. **124**, 044801 (2020).
[26] F. C. Salgado, K. Grafenstein, A. Golub, A. Döpp, A. Eckey, D. Hollatz, C. Müller, A. Seidel, D. Seipt, S. Karsch *et al.*, New J. Phys. **23**, 105002 (2021).
[27] B. King, N. Elkina, and H. Ruhl, Phys. Rev. A **87**, 042117 (2013).
[28] Y.-F. Li, R. Shaisultanov, Y.-Y. Chen, F. Wan, K. Z. Hatsagortsyan, C. H. Keitel, and J.-X. Li, Phys. Rev. Lett. **124**, 014801 (2020).
[29] F. Wan, Y. Wang, R.-T. Guo, Y.-Y. Chen, R. Shaisultanov, Z.-F. Xu, K. Z. Hatsagortsyan, C. H. Keitel, and J.-X. Li, Phys. Rev. Res. **2**, 032049 (2020).
[30] D. Seipt, C. P. Ridgers, D. D. Sorbo, and A. G. R. Thomas, New J. Phys. **23**, 053025 (2021).
[31] D. Seipt, C. P. Ridgers, D. D. Sorbo, and A. G. R. Thomas, New J. Phys. **24**, 029501 (2022).
[32] V. I. Ritus, J. Russ. Laser Res. **6**, 497 (1985).
[33] D. Seipt and B. King, Phys. Rev. A **102**, 052805 (2020).

[34] A. Fedotov, A. Ilderton, F. Karbstein, B. King, D. Seipt, H. Taya, and G. Torgrimsson, Phys. Rep. **1010**, 1 (2023).
[35] C. N. Harvey, A. Ilderton, and B. King, Phys. Rev. A **91**, 013822 (2015).
[36] A. Di Piazza, M. Tamburini, S. Meuren, and C. H. Keitel, Phys. Rev. A **98**, 012134 (2018).
[37] A. Ilderton, B. King, and D. Seipt, Phys. Rev. A **99**, 042121 (2019).
[38] A. Di Piazza, M. Tamburini, S. Meuren, and C. H. Keitel, Phys. Rev. A **99**, 022125 (2019).
[39] B. King, Phys. Rev. A **101**, 042508 (2020).
[40] T. Heinzl, B. King, and A. J. MacLeod, Phys. Rev. A **102**, 063110 (2020).
[41] T. G. Blackburn and B. King, Eur. Phys. J. C **82**, 44 (2022).
[42] T. G. Blackburn, A. J. MacLeod, and B. King, New J. Phys. **23**, 085008 (2021).
[43] M. Turner, S. S. Bulanov, C. Benedetti, A. J. Gonsalves, W. P. Leemans, K. Nakamura, J. van Tilborg, C. B. Schroeder, C. G. R. Geddes, and E. Esarey, Eur. Phys. J. D **76**, 205 (2022).
[44] K. Yokoya and P. Chen, Lect. Notes Phys. **400**, 415 (1992).
[45] A. Hartin, Int. J. Mod. Phys. A **33**, 1830011 (2018).
[46] D. Y. Ivanov, G. L. Kotkin, and V. G. Serbo, Eur. Phys. J. C **36**, 127 (2004).
[47] B. King and S. Tang, Phys. Rev. A **102**, 022809 (2020).
[48] S. Tang, B. King, and H. Hu, Phys. Lett. B **809**, 135701 (2020).
[49] S. Tang, Phys. Rev. D **105**, 056018 (2022).
[50] Y. Gao and S. Tang, Phys. Rev. D **106**, 056003 (2022).
[51] G. Torgrimsson, New J. Phys. **23**, 065001 (2021).
[52] B. King, Phys. Rev. D **103**, 036018 (2021).
[53] S. Tang and B. King, Phys. Rev. D **104**, 096019 (2021).
[54] A. Di Piazza, C. Müller, K. Z. Hatsagortsyan, and C. H. Keitel, Rev. Mod. Phys. **84**, 1177 (2012).
[55] A. Gonoskov, T. G. Blackburn, M. Marklund, and S. S. Bulanov, Rev. Mod. Phys. **94**, 045001 (2022).
[56] A. R. Bell and J. G. Kirk, Phys. Rev. Lett. **101**, 200403 (2008).
[57] J. G. Kirk, A. R. Bell, and I. Arka, Plasma Phys. Controlled Fusion **51**, 085008 (2009).
[58] E. N. Nerush, I. Yu. Kostyukov, A. M. Fedotov, N. B. Narozhny, N. V. Elkina, and H. Ruhl, Phys. Rev. Lett. **106**, 035001 (2011).
[59] N. V. Elkina, A. M. Fedotov, I. Yu. Kostyukov, M. V. Legkov, N. B. Narozhny, E. N. Nerush, and H. Ruhl, Phys. Rev. ST Accel. Beams **14**, 054401 (2011).
[60] S. Tang, M. A. Bake, H.-Y. Wang, and B.-S. Xie, Phys. Rev. A **89**, 022105 (2014).
[61] A. Gonoskov, A. Bashinov, S. Bastrakov, E. Efimenko, A. Ilderton, A. Kim, M. Marklund, I. Meyerov, A. Muraviev, and A. Sergeev, Phys. Rev. X **7**, 041003 (2017).
[62] A. S. Samsonov, E. N. Nerush, and I. Y. Kostyukov, Sci. Rep. **9**, 11133 (2019).
[63] A. Sampath and M. Tamburini, Phys. Plasmas **25**, 083104 (2018).
[64] C. Harvey, T. Heinzl, and A. Ilderton, Phys. Rev. A **79**, 063407 (2009).
[65] J. S. Toll, Ph.D. thesis, Princeton University, 1952.
[66] H. J. Korsch, A. Klumpp, and D. Witthaut, J. Phys. A **39**, 14947 (2006).
[67] E. Lötstedt and U. D. Jentschura, Phys. Rev. E **79**, 026707 (2009).
[68] A. I. Titov, H. Takabe, B. Kämpfer, and A. Hosaka, Phys. Rev. Lett. **108**, 240406 (2012).
[69] T. Nousch, D. Seipt, B. Kämpfer, and A. Titov, Phys. Lett. B **715**, 246 (2012).